Available online at www.sciencedirect.com
SCIENCE DIRECT®
Journal of Computational and Applied Mathematics 176 (2005) 179–201
JOURNAL OF COMPUTATIONAL AND APPLIED MATHEMATICS
www.elsevier.com/locate/cam

Solution of vector Stefan problems with cross-diffusion

F.J. Vermolen*, C. Vuik

Department of Applied Mathematical Analysis, Delft University of Technology, Mekelweg 4, 2628 CD Delft, the Netherlands

Received 20 January 2004; received in revised form 1 July 2004

Abstract

A general model for the dissolution of particles in multi-component alloys is proposed and analyzed. The model is based on diffusion equations with cross-terms for the several species, combined with a Stefan condition as the equation of motion of the interface between the particle and diffusive phase. Several numerical schemes for the solution of the Stefan problem are proposed and compared. It turns out that diagonalization is useful for numerical purposes. However, for the case of position-dependent diffusion coefficients one has to use a different scheme. Here, we analyze stability and workload of several time integration methods.

Keywords: Multi-component alloy; Particle dissolution; Cross-diffusion; Vector-valued Stefan problem; Numerical solution; Time-integration

1. Introduction

In the thermal processing of both ferrous and nonferrous alloys, homogenization of the as-cast microstructure by annealing at such a high temperature that unwanted precipitates are fully dissolved, is required to obtain a microstructure suited to undergo heavy plastic deformation as an optimal starting condition for a subsequent precipitation hardening treatment. Such a homogenization treatment, to name just a few examples, is applied in hot-rolling of Al killed construction steels, HSLA steels, all engineering steels, as well as aluminum extrusion alloys. Although precipitate dissolution and growth are not the only metallurgical processes taking place, these are often the most critical of the occurring processes. The minimum temperature at which the annealing should take place can be determined from thermodynamic

* Corresponding author. Tel.: +31-15-278-1833; fax: +31-15-278-7209.
E-mail address: F.J.Vermolen@math.tudelft.nl (F.J. Vermolen).

0377-0427/$ - see front matter © 2004 Elsevier B.V. All rights reserved.
doi:10.1016/j.cam.2004.07.011

analysis of the phases present. The minimum annealing time at this temperature, however, is not a constant but depends on particle size, particle geometry, particle concentration, overall composition, etc.

Due to the scientific and industrial relevance of being able to predict the kinetics of particle dissolution and growth, many models of various complexity have been presented and experimentally validated. In recent years the simpler models covering binary and ternary alloys have been extended to cover multi-component particles. These advanced models cover a range of physical assumptions concerning the dissolution conditions and the initial microstructure. The nature of the Stefan problem changes here: we consider the simultaneous diffusion of several alloying elements. This gives rise to a nonlinear problem to solve. For a review and more physical background of this problem we refer to [21].

We will put the present paper into perspective of our previous papers on vector-valued Stefan problems. In [18] the full numerical method for a vector-valued Stefan problem with two alloying elements (i.e., a ternary alloy) is presented. Further, numerical consequences of the presence of two separate moving interfaces are analyzed there. In [19] a generalization to multi-component alloys is made. Further, some mathematical properties concerning mass-conservation and existence of solutions are analyzed there. In the preceding two papers the effects of cross-diffusion have been disregarded. In [21] we consider some metallurgical implications from cross-diffusion on the rate of dissolution. This was a parameter study. In [22] we present a self-similar solution based on Boltzmann transformation for the vector-valued Stefan problem with cross-diffusion for an unbounded planar domain. This solution is used to check numerically obtained results. The present paper consists of a comparison of several numerical methods to solve the vector-valued Stefan problem with cross-diffusion. Also as an alternative to the Newton method with approximated Jacobian, which converges fast but for which each iteration step is expensive, we present the use of Picard's method to solve the nonlinear problem.

In this paper, we study the performance of several numerical methods in terms of numerical stability and efficiency for a model of particle dissolution and growth in multi-component alloys, i.e., alloys with several alloying elements. The model is based on a vector-valued Stefan problem where the effects of cross-diffusion are taken into account. A self-similarity solution for a one-dimensional geometry is presented in [22]. The present paper is organized as follows: The model equations are introduced first. Subsequently, we propose several numerical approaches. This is followed by a qualitative analysis in terms of numerical stability and efficiency. Some numerical experiments are given and finally the conclusions are presented.

2. The model

The as-cast microstructure of the alloy is simplified into a representative cell containing a diffusive phase $\Omega(t)$ and a single particle of a specific form, size and location. To avoid confusion we will refer to the diffusive phase as the Ω-phase. The particle is allowed to dissolve or grow due to diffusion of several chemical elements in the Ω-phase. We assume that only diffusion determines the rate of growth or dissolution. In the present paper, we take the effects from cross-diffusion into account. The boundary between the particle and the Ω-phase is referred to as the interface, denoted by $S(t)$. Hence, in the Ω-phase we have from Fick's second law

$$\frac{\partial c_i}{\partial t} = \sum_{j=1}^{n_s} D_{ij} \Delta c_j \quad \text{for } (x, y) \in \Omega(t), \quad t > 0. \tag{1}$$

In (1) c_i denotes the concentration of alloying element for $i \in \{1, \ldots, n_s\}$. The coefficients D_{ij} are the diffusion coefficients, where D_{ij} for $i \neq j$ denote cross-diffusion coefficients. If $D_{ij} = 0$ for $i \neq j$ then the classical diffusion equations are recovered. Further, we assume that the concentrations in the particle, c_i^{part}, are given and fixed at all stages of the calculations. This directly follows from the assumption that the particle remains stoichiometric during the process, which is in line with the treatment by Reiso et al. [17] among others. Initially, a concentration profile is given in the Ω-phase

$$c_i(x, y, 0) = c_i^0(x, y) \quad \text{for } (x, y) \in \Omega(0). \tag{2}$$

The initial position of the interface is known and denoted by $S(0)$. At a boundary not being a moving interface, we assume no flux through it, i.e.,

$$\frac{\partial c_i}{\partial v} = 0 \quad \text{for } (x, y) \in \Gamma(t), \quad t > 0. \tag{3}$$

In (3) v represents the outward unit normal vector of $\Omega(t)$. Furthermore, at the moving interface $S(t)$ we denote c_i^{sol}, for each alloying element, i.e.,

$$c_i(x, y, t) = c_i^{\text{sol}} \quad \text{for } (x, y) \in S(t), \quad t > 0. \tag{4}$$

We consider the dissolution or growth of a stoichiometric particle where we denote the chemical species by Sp_i, $i \in \{1, \ldots, n_s\}$, where Sp_{n_s+1} is the 'original' solvent metallic Ω-phase in which the particle is allowed to grow or dissolve. We denote the stoichiometry of the particle by $(\text{Sp}_1)_{m_1}(\text{Sp}_2)_{m_2}(\ldots)(\text{Sp}_{n_s})_{m_{n_s}}$. The numbers $m_1, \ldots, m_{n_s}$ are stoichiometric constants. For the interface concentrations c_i^{sol} we use the hyperbolic relationship

$$(c_1^{\text{sol}})^{m_1}(c_2^{\text{sol}})^{m_2}(\ldots)(c_{n_s}^{\text{sol}})^{m_{n_s}} = K, \tag{5}$$

where K is known and may depend on time t for a nonisothermal Stefan problem. However, in the present study we take it as a constant. The above relation follows from thermodynamical arguments, see for instance [10] for a justification. From a local mass balance, the outward normal component of the interface velocity, v_v, is described by

$$(c_i^{\text{part}} - c_i^{\text{sol}})v_v = \sum_{j=1}^{n_s} D_{ij} \frac{\partial c_j}{\partial v} \quad \text{for } (x, y) \in S(t), \quad t > 0. \tag{6}$$

The above relation is referred to as the Stefan condition and v denotes the unit outward normal vector of $\Omega(t)$ at $S(t)$. Since the above relation holds for $i \in \{1, \ldots, n_s\}$, the interface velocity is eliminated if $c_i^{\text{part}} \neq c_i^{\text{sol}}$, hence

$$\sum_{k=1}^{n_s} \frac{D_{ik}}{c_i^{\text{part}} - c_i^{\text{sol}}} \frac{\partial c_k}{\partial v} = \sum_{k=1}^{n_s} \frac{D_{jk}}{c_j^{\text{part}} - c_j^{\text{sol}}} \frac{\partial c_k}{\partial v} \quad \text{for } (x, y) \in S(t), \quad t > 0. \tag{7}$$

Above-formulated problem falls within the class of Stefan-problems, i.e., diffusion with a moving boundary. Since we consider simultaneous diffusion of several chemical elements, it is referred to as a

'vector-valued Stefan problem'. The unknowns in above equations are the concentrations c_i, interfacial concentrations c_i^{sol} and the interfacial position $S(t)$. All concentrations are nonnegative. The coupling exists in both the diffusion equations (1), motion equations (7) and the values of the concentrations at the interfaces between the particle and diffusive phase (5). We note here that the equations for the 'linear case', where the boundary is fixed, are asymptotically stable if and only if $\Re\{\mathrm{eig}(D)\} > 0$. Hence only this case is considered in the present study. For a mathematical overview of Stefan problems we refer to the textbooks of Crank [5], Meirmanov et al. [13], Chadam and Rasmussen [3] and Visintin [23], between others.

3. Numerical approaches

In general, situations we are not able to give an analytical solution for the vector-valued Stefan problem with cross-diffusion and hence a numerical method is used. The Stefan problem considered in this paper contains two difficulties

- the computation of the moving interface;
- the occurrence of the cross-diffusion terms.

Our main interest is to give an accurate discretization for this Stefan problem. Therefore, we use the classical moving grid method of Murray and Landis [14] to discretize the diffusion equations. For a survey of other methods, we refer to [4,8,9,11,16]. The methods in the present paper are based on finite differences with one spatial co-ordinate. A characteristic of the moving grid method is that the interface position co-incides with a nodal point at each time-step. For completeness, we give a rough description of the algorithm, which is the backbone of all the methods that we present in the present paper:

1. Compute the concentration profile from Fick's second law (1), using a convective derivative, taking into account the mesh displacement at each time-step;
2. Predict the interface position by use of the Stefan condition (6);
3. Redistribute the grid such that the interface position is a nodal point.
4. Return to step 1.

In this section two numerical methods are presented. The first method is based on diagonalization of the diffusion matrix. Then, it is straightforward to use an implicit time integration method, which is unconditionally stable. For the first method, the vector-valued Stefan problem is solved by using the method presented in [19], except for the more complicated expression for the transformed interface concentrations. The second method solves the diffusion equations with cross-diffusion terms directly. Here, we will give the discretization equations of three time integration methods. We note that the integration of the vector-valued Stefan problem by the use of the diagonalization method (i.e., the first method) can be recovered from the presentation of the second method by setting the off-diagonal coefficients in the diffusion matrix to zero. A fully implicit time integration can be used then, however it is less straightforward than in the first method. We conclude this section with the description of the application of the Newton method with Finite Differences and (relaxed) Picard iteration method to solve the nonlinear problem for the concentrations at the interface.

3.1. The diagonalization approach

First, the eigenvalues and eigenvectors of the diffusion matrix are computed for the transformation of the concentration. The particle concentrations are also transformed and the hyperbolic relation (5) between the interfacial concentrations changes.

We change to a vector notation of the equations in the vector-valued Stefan problem. We define the vectors $\underline{c} := (c_1, c_2, \ldots, c_{n_s})^{\mathrm{T}}, \underline{c}^p := (c_1^{\mathrm{part}}, c_2^{\mathrm{part}}, \ldots, c_{n_s}^{\mathrm{part}})^{\mathrm{T}}, \underline{c}^s := (c_1^{\mathrm{sol}} c_2^{\mathrm{sol}}, \ldots, c_{n_s}^{\mathrm{sol}})^{\mathrm{T}}$. We assume that the matrix D is constant with positive real eigenvalues. We use the Decomposition Theorem to diagonalize D, i.e., there exists for D a nonsingular $P \in \mathbb{R}^{n_s \times n_s}$ such that $\Lambda = P^{-1} D P$. Here Λ is a diagonal matrix with the eigenvalues of D if D is diagonalizable (i.e., if D has n_s linearly independent eigenvectors). If D is not diagonalizable then Λ is a block Jordan matrix and P consists of the generalized eigenvectors of D (see for instance Birkhoff and MacLane [2]). Changing Eqs. (1) and (6) to a vector-notation gives:

$$\frac{\partial \underline{c}}{\partial t} = D \Delta \underline{c} \quad \text{for } (x, y) \in \Omega(t), \quad t > 0, \tag{8}$$

$$(\underline{c}^p - \underline{c}^s) v_v = D \frac{\partial \underline{c}}{\partial v} \quad \text{for } (x, y) \in S(t), \quad t > 0. \tag{9}$$

After defining the transformed concentrations by

$$\begin{aligned} &\underline{u} := P^{-1} \underline{c}, \quad \underline{u}^s := P^{-1} \underline{c}^s, \\ &\underline{u}^p := P^{-1} \underline{c}^p, \quad \underline{u}^0 := P^{-1} \underline{c}^0, \end{aligned} \tag{10}$$

the diffusion equations and equation of motion change into

$$\frac{\partial \underline{u}}{\partial t} = \Lambda \Delta \underline{u} \quad \text{for } (x, y) \in \Omega(t), \quad t > 0, \tag{11}$$

$$(\underline{u}^p - \underline{u}^s) v_v = \Lambda \frac{\partial \underline{u}}{\partial v} \quad \text{for } (x, y) \in S(t), \quad t > 0. \tag{12}$$

Note that if D is diagonalizable then there is no coupling in the diffusion equations via cross-terms of Λ. The coupling between the various chemical species expressed in $\underline{u}$ remains via Eq. (12) and the hyperbolic relation for $c_1^{\mathrm{sol}}, \ldots, c_{n_s}^{\mathrm{sol}}$ in Eq. (5). Eq. (5) changes due to transformations (10) into

$$\left(\sum_{j=1}^{n_s} p_{1j} u_j^s \right)^{m_1} \left(\sum_{j=1}^{n_s} p_{2j} u_j^s \right)^{m_2} (\ldots) \left(\sum_{j=1}^{n_s} p_{nj} u_j^s \right)^{m_{n_s}} = K. \tag{13}$$

Although this last relation is more complicated, the analysis and numerical solution procedure are facilitated. For the analytical solutions of the cross-diffusion problem we refer to [22] and Atkinson et al. [1]. The self-similar solution is used for the validation of the numerical solution at the early stages of the model.

Whether or not the diffusion matrix is diagonalizable, we always have at least one uncoupled diffusion equation for each eigenvalue of D and hence there is an entry of the transformed concentrations u_i for which the diffusion equation is uncoupled. This implies that if one of the eigenvalues is negative, or has a negative real part, then we face a diffusion equation with a negative diffusion coefficient, which is well-known to be ill-posed. This motivates the requirement that the eigenvalues of D must be positive or have a

positive real part. Further, complex eigenvalues give rise to oscillatory solutions for the concentrations. In the present work, we limit ourselves to situations with real and positive eigenvalues. An analytical study, where also the case of a singular diffusion matrix is treated, is in progress, the preliminary results are described in [20]. After diagonalization of the diffusion matrix we apply the same discretization procedure as for the vector-valued Stefan problem without cross-diffusion. For completeness we briefly summarize the method, more details on the method can be found in [19].

For the determination of the interface velocity a discrete version of the Stefan condition (12) is used. Since Eq. (12) holds for all components, elimination of the interface velocity leads to $n_s - 1$ boundary equations for the concentrations. These equations are supplemented with Eq. (13) to get a solution of physical interest. Subsequently, the system of equations is solved by the use of a zero-point method to be described later in this section.

In the present study, we limit ourselves to cases where D is a constant matrix. For completeness, we write some remarks on the case that the diffusion matrix depends on time and is diagonalizable, i.e., $D = D(t) = P(t)\Lambda(t)P^{-1}(t)$. Then, we have

$$\frac{\partial \underline{c}}{\partial t} = P(t)\Lambda(t)P^{-1}(t)\Delta\underline{c}. \tag{14}$$

Hence after left-multiplication with P^{-1}, this changes into

$$P^{-1}(t)\,\frac{\partial \underline{c}}{\partial t} = \Lambda(t)\Delta P^{-1}(t)\underline{c}. \tag{15}$$

In the last step we used that the P does not depend on position and hence commutes with the Laplacian. Defining $\underline{u} := P^{-1}(t)\underline{c}$, we see from the product rule for differentiation that Eq. (11) does not hold any longer. The only case of a time-dependent diffusion matrix for which Eq. (11) still holds is if D can be written by $D = D(t) = P^{-1}\Lambda(t)P$.

For the discrete problem the following notations are introduced. Denote the diffusion matrix, transformation matrix and the diagonal matrix with the eigenvalues at time-step j by D_j, P_j and Λ_j, respectively. Then we obtain the following discrete version for Euler backward time integration in matrix-notation:

$$\underline{c}^{j+1} = \underline{c}^{j} + \Delta t\, D_{j+1}\Delta\underline{c}^{j+1} = \underline{c}^{j} + \Delta t\, P_{j+1}\Lambda_{j+1}\Delta P^{-1}_{j+1}\underline{c}^{j+1}. \tag{16}$$

Left-multiplication of the above equation by P^{-1}_{j+1} gives

$$P^{-1}_{j+1}\underline{c}^{j+1} = P^{-1}_{j+1}\underline{c}^{j} + \Delta t\,\Lambda_{j+1}\Delta P^{-1}_{j+1}\underline{c}^{j+1}. \tag{17}$$

In the above equation the concentrations of the several species are decoupled by the diagonalization. However, if the transformation of the concentrations is defined by $P_j^{-1}\underline{c}^{j} =: \underline{u}^{j}$, then still $\underline{c}^{j}$ is needed. Hence it is possible to treat $D(t)$ by diagonalization, however, at each time-step we need to carry out the transformation and inverse transformation of the concentrations at each grid-node. We summarize this in the following remark:

Remark 1. If the diffusion matrix depends on time then at each time step the diagonalization argument can be applied successfully. However, the transformation (and its inverse) has to be applied at each time-step and grid-node, which makes the method expensive.

3.2. The direct numerical method

In this section, we describe the direct numerical solution of the vector-valued Stefan problems. The description is for a situation in which we deal with one spatial co-ordinate on interval $[0,\ M]$, where $M > 0$ denotes the end-point of the domain of computation. We consider the particle with fixed concentration as given by $0 \leqslant x \leqslant S(t)$ and the diffusive phase given by $S(t) < x \leqslant M$. First, we describe the discretization of the diffusion equations for which we remark that we refer to [19] for more details. Subsequently, the discrete boundary conditions at the moving interface and the solution procedures to solve the resulting nonlinear problem are treated. Finally, the adaptation of the moving boundary is described.

3.2.1. Discretization of the interior region

We use a finite difference method with a Euler forward or backward or IMEX time integration to solve the diffusion equation in the inner region. For completeness we give the equations for the discretization of the inner region for the three time integration methods only for the case of planar (rectangular) geometry and an equidistant grid in which we consider two diffusing species only. Let Δx, Δt, $c_{k,i}^{j}$ and x_i^j, respectively, denote the grid-spacing, time-step, numerical approximation of the concentration of species k at grid-node i at time $j\Delta t$ and position of grid-node i at time $j\Delta t$. Then, for the Euler forward (explicit) method one obtains

$$\begin{aligned}
&\frac{c_{1,i}^{j+1}-c_{1,i}^{j}}{\Delta t}-\frac{x_i^{j+1}-x_i^{j}}{\Delta t}\,\frac{c_{1,i+1}^{j}-c_{1,i-1}^{j}}{2\Delta x}\\
&\quad= D_{11}\,\frac{c_{1,i-1}^{j}-2c_{1,i}^{j}+c_{1,i+1}^{j}}{\Delta x^2}+D_{12}\,\frac{c_{2,i-1}^{j}-2c_{2,i}^{j}+c_{2,i+1}^{j}}{\Delta x^2},\\
&\frac{c_{2,i}^{j+1}-c_{2,i}^{j}}{\Delta t}-\frac{x_i^{j+1}-x_i^{j}}{\Delta t}\,\frac{c_{2,i+1}^{j}-c_{2,i-1}^{j}}{2\Delta x}\\
&\quad= D_{21}\,\frac{c_{1,i-1}^{j}-2c_{1,i}^{j}+c_{1,i+1}^{j}}{\Delta x^2}+D_{22}\,\frac{c_{2,i-1}^{j}-2c_{2,i}^{j}+c_{2,i+1}^{j}}{\Delta x^2}.
\end{aligned}\tag{18}$$

Whereas for the Euler backward (implicit) method one gets

$$\begin{aligned}
&\frac{c_{1,i}^{j+1}-c_{1,i}^{j}}{\Delta t}-\frac{x_i^{j+1}-x_i^{j}}{\Delta t}\,\frac{c_{1,i+1}^{j}-c_{1,i-1}^{j}}{2\Delta x}\\
&\quad= D_{11}\,\frac{c_{1,i-1}^{j+1}-2c_{1,i}^{j+1}+c_{1,i+1}^{j+1}}{\Delta x^2}+D_{12}\,\frac{c_{2,i-1}^{j+1}-2c_{2,i}^{j+1}+c_{2,i+1}^{j+1}}{\Delta x^2},\\
&\frac{c_{2,i}^{j+1}-c_{2,i}^{j}}{\Delta t}-\frac{x_i^{j+1}-x_i^{j}}{\Delta t}\,\frac{c_{2,i+1}^{j}-c_{2,i-1}^{j}}{2\Delta x}\\
&\quad= D_{21}\,\frac{c_{1,i-1}^{j+1}-2c_{1,i}^{j+1}+c_{1,i+1}^{j+1}}{\Delta x^2}+D_{22}\,\frac{c_{2,i-1}^{j+1}-2c_{2,i}^{j+1}+c_{2,i+1}^{j+1}}{\Delta x^2}.
\end{aligned}\tag{19}$$

Finally, for the IMEX time integration, we have the following:

$$\begin{aligned}
&\frac{c_{1,i}^{j+1}-c_{1,i}^{j}}{\Delta t}-\frac{x_i^{j+1}-x_i^{j}}{\Delta t}\,\frac{c_{1,i+1}^{j}-c_{1,i-1}^{j}}{2\Delta x}\\
&\quad=D_{11}\,\frac{c_{1,i-1}^{j+1}-2c_{1,i}^{j+1}+c_{1,i+1}^{j+1}}{\Delta x^2}+D_{12}\,\frac{c_{2,i-1}^{j}-2c_{2,i}^{j}+c_{2,i+1}^{j}}{\Delta x^2},\\
&\frac{c_{2,i}^{j+1}-c_{2,i}^{j}}{\Delta t}-\frac{x_i^{j+1}-x_i^{j}}{\Delta t}\,\frac{c_{2,i+1}^{j}-c_{2,i-1}^{j}}{2\Delta x}\\
&\quad=D_{21}\,\frac{c_{1,i-1}^{j}-2c_{1,i}^{j}+c_{1,i+1}^{j}}{\Delta x^2}+D_{22}\,\frac{c_{2,i-1}^{j+1}-2c_{2,i}^{j+1}+c_{2,i+1}^{j+1}}{\Delta x^2}.
\end{aligned}\tag{20}$$

We note that it is straightforward to deal with cylindrical and spherical geometries as well. Further, a geometrically distributed grid has been implemented where a mesh refinement is applied for the nodes near the interface and the procedure is easily extended to more diffusing chemical elements. This is described in more detail in [19]. From the Eqs. (18)–(20) it can be seen that an explicitly treated centrally discretized convection term due to grid-movement is included. We use a virtual grid-point near the moving boundary. The distance between the virtual node and the interface is chosen equal to the distance between the interface and the first grid-node.

3.2.2. Discrete boundary conditions at the interface

We define the discrete approximation of the concentration as $c_{k,i}^{j}$, where j, k and i, respectively, denote the time-step, the index of the chemical (alloying) element and gridnode. The virtual gridnode near the moving interface and the gridnode at the interface, respectively, have indices $i=-1$ and 0. At the moving interface, we obtain from discretization of the Stefan condition for $k\in\{1,\dots,n_s-1\}$

$$\frac{1}{c_k^{\mathrm{part}}-c_k^{\mathrm{sol}}}\left\{\sum_{p=1}^{n_s}D_{k,p}\,\frac{c_{p,1}^{j+1}-c_{p,-1}^{j+1}}{2\Delta x}\right\}=\frac{1}{c_{k+1}^{\mathrm{part}}-c_{k+1}^{\mathrm{sol}}}\left\{\sum_{p=1}^{n_s}D_{k+1,p}\,\frac{c_{p,1}^{j+1}-c_{p,-1}^{j+1}}{2\Delta x}\right\}.\tag{21}$$

Note that the concentration profile of each chemical species is determined by the value of the interfacial concentration. Hence, all the concentrations that appear in the above equation and Eqs. (18)–(20) depend on the interface concentrations. Above equation can be re-arranged into a zero-point problem for the interface concentrations of the chemical elements. All interfacial concentrations satisfy the hyperbolic relation (5). Combination of the above relation (21) and (5), gives for $k\in\{1,\dots,n_s-1\}$

$$\begin{aligned}
f_k(c_1^{\mathrm{sol}},\dots,c_{n_s}^{\mathrm{sol}})=&(c_{k+1}^{\mathrm{part}}-c_{k+1}^{\mathrm{sol}})\sum_{p=1}^{n_s}D_{k,p}(c_{p,1}^{j+1}-c_{p,-1}^{j+1})\\
&-(c_k^{\mathrm{part}}-c_k^{\mathrm{sol}})\sum_{p=1}^{n_s}D_{k+1,p}(c_{p,1}^{j+1}-c_{p,-1}^{j+1})=0
\end{aligned}$$

and the equation

$$f_{n_s}(c_1^{\mathrm{sol}}, \ldots, c_{n_s}^{\mathrm{sol}}) = (c_1^{\mathrm{sol}})^{m_1}(c_2^{\mathrm{sol}})^{m_2}(\ldots)(c_{n_s}^{\mathrm{sol}})^{m_{n_s}} - K = 0.$$

Here the unknowns $c_1^{\mathrm{sol}}, \ldots, c_{n_s}^{\mathrm{sol}}$ are to obtained from previous n_s equations.

3.2.3. Adaptation of the moving boundary

The moving interface is adapted according to a second-order discretized version of the Stefan condition (6) where the virtual gridnode is used. In [18] the forward (explicit) Euler and Trapezium time integration methods for the moving boundary condition are described and compared. It was found that the (implicit) Trapezium method was superior in accuracy. Furthermore, we update the interfacial concentrations in each Trapezium step. Hence, the work per time-iteration remains the same for both time-integration methods. Therefore, the Trapezium rule is used to determine the interfacial position as a function of time. We terminate the iteration at time $(j+1)\Delta t$ when sufficient accuracy is reached, i.e., let ε be the accuracy, then we stop at iteration $p+1$ when the inequality

$$\sum_{k=1}^{n_s} |c_k^{\mathrm{sol}}(p+1) - c_k^{\mathrm{sol}}(p)| + \frac{|S^{j+1}(p+1) - S^{j+1}(p)|}{S^j - M} < \varepsilon$$

holds. Here S^j denotes the discrete approximation of the interfacial position at time-step j. We finally remark that a numerical solution for diffusion in ternary alloys including cross-diffusion for fixed boundaries can also be found in Naumann and Savoca [15]. They used an argument based on cross-diffusion to avoid the need of dealing with composition-dependent diffusion coefficients. This is motivated by the occurrence of negative concentrations otherwise.

3.3. Solution of the nonlinear problem

To approximate a root for the 'vector-function' $\mathbf{f} = (f_1, \ldots, f_{n_s})$, in both the first and second method, we use a numerical method. We compare the solution by using Newton's method with finite differences approximated Jacobian to the solution obtained by the Picard iterations. Let $\underline{z} := (c_1^{\mathrm{sol}}, \ldots, c_{n_s}^{\mathrm{sol}})^{\mathrm{T}}$, then

$$\underline{z}^{k+1} = \underline{z}^k - J^{-1}(\underline{z}^k)\underline{f}(\underline{z}^k),$$

where J denotes the discretized Jacobian matrix, where central differences are used for the determination of the derivatives of the first $n_s - 1$ equations. The iteration is terminated when sufficient accuracy is reached. This is explained in more detail in [19]. Note that for each Newton iteration five evaluations of the concentration profiles are needed. Further, the initial guess must be close to the solution and the convergence of the Newton iteration scheme is quadratic. Hence, if the method converges, then convergence is fast. The 'fixed point' iteration scheme is based on

$$\underline{z}^{k+1} = \underline{g}(\underline{z}^k),$$

where the vector-function $\underline{g}$ is defined as:

$$c_1^{\mathrm{sol}} = g_1 := \frac{K}{(c_1^{\mathrm{sol}})^{m_1-1}(c_2^{\mathrm{sol}})^{m_2}(\ldots)(c_{n_s}^{\mathrm{sol}})^{m_{n_s}}},$$

$$c_{k+1}^{\mathrm{sol}} = g_{k+1} := c_{k+1}^{\mathrm{part}} - \frac{(c_k^{\mathrm{part}} - c_k^{\mathrm{sol}})\sum_{p=1}^{n_s} D_{k+1,p}(c_{p,1}^{j+1} - c_{p,-1}^{j+1})}{\sum_{p=1}^{n_s} D_{k,p}(c_{p,1}^{j+1} - c_{p,-1}^{j+1})}, \quad k \in \{1, \ldots, n_s - 1\}.$$

A disadvantage of the Picard-iteration scheme is that the convergence is linear. However, only one evaluation of the concentration profile is needed per iteration, hence cost per iteration is reduced five times. A criterion for convergence of the Picard iterations is that the spectral radius of the Jacobian of the function $\underline{g}$ should be less than one. For large Δt we observed that the method does not converge and that the spectral radius becomes larger than one. For these cases a Picard iteration scheme with relaxation is used, which reads as

$$\underline{z}^{k+1} = \underline{z}^k + \omega(\underline{g}(\underline{z}^k) - \underline{z}^k),$$

where ω is the relaxation parameter. For some $\omega > 0$ a slightly better convergence is obtained, although not for all $0 < \omega < 1$ the improvement is significant. Further, we see that the error, defined by $\|\underline{z}^{k+1} - \underline{z}^k\|_2$, gets less than 10^{-6} after 31 iterations, whereas for the other simulations a standard maximum number of 20 iterations was used.

4. Comparison between the approaches

In this section, we compare both methods qualitatively in terms of stability and efficiency. First, stability is analyzed for the direct method for several time integration schemes. A stability condition is derived for the cross-diffusion problem with a nonmoving boundary. This criterion can be used as a necessary condition for stability of the numerical solution of the vector-valued Stefan problem. We remark that in, among others, [6] numerical stability of weak and variational methods for a (scalar) moving boundary problem, is treated. However, a vector-valued Stefan problem is not considered there.

Subsequently, we compare the efficiency of the two methods qualitatively. Numerical experiments to support the findings are given in the next section. In this section, we restrict ourselves to a vector cross diffusion problem with fixed boundaries. Two methods can be used. First, if the diffusion matrix is constant the diagonalization argument can be used (see Section 3). If this assumption does not hold a direct numerical method for the diffusion equations should be used. In the first method (with diagonalization) the stability properties of the time integration are well-known.

4.1. Stability of the direct method for the linear cross diffusion problem

Here, we investigate the stability properties for various time integration methods for the coupled equations. For the stability analysis we again assume that D is constant. The treatment is for finite differences, volumes and elements with fixed boundaries. For finite element methods, it follows that the stiffness matrix (the discretized Laplacian) is always symmetric positive definite. However, Eqs. (27) change due to the mass-matrix M that appears in the finite element formulation

$$\begin{pmatrix} M & 0 \\ 0 & M \end{pmatrix} \frac{\mathrm{d}\underline{c}}{\mathrm{d}t} = \begin{pmatrix} D_{11}L & D_{12}L \\ D_{21}L & D_{22}L \end{pmatrix} \begin{pmatrix} \underline{c}_1 \\ \underline{c}_2 \end{pmatrix}. \tag{22}$$

Since M is nonsingular, the above equation is re-written as

$$\frac{\mathrm{d}\underline{c}}{\mathrm{d}t} = \begin{pmatrix} D_{11}M^{-1}L & D_{12}M^{-1}L \\ D_{21}M^{-1}L & D_{22}M^{-1}L \end{pmatrix} \begin{pmatrix} \underline{c}_1 \\ \underline{c}_2 \end{pmatrix}. \tag{23}$$

Now, we use symmetry and positive definiteness of M (hence $M^{1/2}$ exists) to show that $M^{-1}L$ has negative (real-valued) eigenvalues. Since $M^{-1}L$ is similar to $M^{1/2}M^{-1}LM^{-1/2} = M^{-1/2}LM^{-1/2}$, it can be seen that the eigenvalues of $M^{-1}L$ are real-valued due to symmetry of $M^{-1/2}LM^{-1/2}$. Next, we show that $M^{-1}L$ has negative eigenvalues only. Since $(Lx, x) < 0$ for all $x \neq 0$, we have $(LM^{-1/2}y, M^{-1/2}y) < 0$ for all $y \neq 0$ ($M^{-1/2}$ is nonsingular). Since $M^{-1/2}$ is symmetric, it follows that $(M^{-1/2}LM^{-1/2}y, y) < 0$ for all $y \neq 0$. Combined with symmetry this gives that all eigenvalues of $M^{-1/2}LM^{-1/2}$ are negative. Hence, due to the similarity of $M^{-1}L$ to $M^{-1/2}LM^{-1/2}$, $M^{-1}L$ has negative (real-valued) eigenvalues only. This implies that the stability analysis also applies for finite element methods and that for finite elements the matrix L in the treatment to follow should be replaced by $M^{-1}L$. We consider the time integration of

$$\frac{\partial c_1}{\partial t} = D_{11}\Delta c_1 + D_{12}\Delta c_2, \tag{24}$$

$$\frac{\partial c_2}{\partial t} = D_{21}\Delta c_1 + D_{22}\Delta c_2. \tag{25}$$

Since the Laplacian operator is negative and self-adjoint, we assume that the discretization matrix for Δ, denoted by L, is symmetric and negative definite. Hence, its eigenvalues are negative. Further, we assume that the terms on the main diagonal of D are positive, i.e., $D_{11}, D_{22} > 0$ and $D \in \mathbb{R}^{2\times 2}$. Then, we write the discretized version as

$$\frac{\mathrm{d}\underline{c}}{\mathrm{d}t} = \begin{pmatrix} D_{11}L & D_{12}L \\ D_{21}L & D_{22}L \end{pmatrix} \begin{pmatrix} \underline{c}_1 \\ \underline{c}_2 \end{pmatrix} =: A\underline{c}, \tag{26}$$

where we use the following notation for N gridpoints:

$$\underline{c}_1 := (c_{1,1}\ c_{1,2}\ \ldots\ c_{1,N})^{\mathrm{T}}, \quad \underline{c}_2 := (c_{2,1}\ c_{2,2}\ \ldots\ c_{2,N})^{\mathrm{T}}, \quad \underline{c} = \begin{pmatrix} \underline{c}_1 \\ \underline{c}_2 \end{pmatrix}. \tag{27}$$

We observe that the matrix A in Eq. (26) represents a Kronecker product. For stability of Eq. (25) we require that

$$\Re(\mathrm{eig}(A)) < 0. \tag{28}$$

Let λ be an eigenvalue of L and let μ be an eigenvalue of D, then $\mu\lambda$ is an eigenvalue of A. This assertion can for instance be found in Lancaster [12]. Since L is symmetric and only has negative (real-valued) eigenvalues, this implies in combination with Eq. (28) that we should have

$$\Re(\mathrm{eig}(D)) > 0 \tag{29}$$

in order to have that perturbations in the solution of Eq. (26) decrease if time increases.

Now we analyze the numerical stability of the following time integration methods for Eq. (26):

1. Euler forward time integration,
2. Euler backward time integration,
3. Implicit explicit (IMEX) time integration.

The discretized equations are the same as in (18)–(20), except for the lack of the mesh velocity term in this section of the stability analysis. We describe the first two cases for this vector-valued diffusion for completeness. We remark here that the stability analysis is based on the assumption that the eigenvalues of the discrete Laplacian are negative, i.e., $\lambda < 0$. This is always true if L is symmetric negative definite. We remark here that the analysis is done for the cross-diffusion problem with fixed boundaries.

4.1.1. Euler forward and backward

1. *The Euler forward time integration method* of Eq. (26) is given by

$$\underline{c}^{n+1} = (I + \Delta t A)\underline{c}^{n}. \tag{30}$$

If the eigenvalues of A are real, we obtain the following bound on Δt:

$$\Delta t < \frac{2}{|\lambda_1|\mu_1}, \tag{31}$$

where $|\lambda_1|$ and μ_1, respectively, represent the spectral radius of L and the largest eigenvalue of D. For the case of finite differences with uniform gridsize h in one spatial dimension, Gerschgorin's Theorem delivers the stability criterion

$$\Delta t < \frac{h^2}{2\mu_1}. \tag{32}$$

This stability condition coincides with the stability condition that is obtained if the diagonalization argument is combined with an explicit time integration. If $\mathrm{eig}(D) \notin \mathbb{R}$, we obtain after some algebra

$$\Delta t < \frac{2\Re(\mathrm{eig}(D))}{|\mathrm{eig}(D)|^2|\lambda_1|}. \tag{33}$$

Nauman and Savoca [15] use an Euler forward (explicit) scheme to integrate the system of diffusion equations in time. Hence, their integration is subject to the above condition.

2. *The Euler backward time integration method* of Eq. (26) is given by

$$\underline{c}^{n+1} = \underline{c}^{n} + \Delta t A\underline{c}^{n+1} \;\Leftrightarrow\; (I - \Delta t A)\underline{c}^{n+1} = \underline{c}^{n}. \tag{34}$$

Since we only consider cases in which $\Re(\mu) > 0$ and $\lambda < 0$, it appears that the Euler backward method is unconditionally stable. The use of Euler backward time integration guarantees the stability of the numerical solution. However, the use of this method gives a large discretization matrix A, which makes each time-integration step expensive, especially for higher dimensional problems.

IMEX time integration: We do the analysis for a 2×2 diffusion matrix where both D_{12} and D_{21} are nonzero. Further, the boundaries are fixed here. In order to combine the advantages of the stability of the Euler backward method with the low cost per iteration step if the Euler forward method is used, we

analyze the IMEX method as given in Eq. (35). If one of the cross-diffusion coefficients is zero, then the diffusion equation with the zero cross term can be integrated by the direct use of Euler backward to obtain its concentration profile. Subsequently, this concentration can be substituted into the other diffusion equation to obtain the other concentration by the use of Euler backward. Hence the use of IMEX is not necessary to decrease the cost per time iteration.

In the IMEX time integration we consider the implicit treatment of the terms of the diffusion matrix that are on the main diagonal and explicit treatment of the off-diagonal terms, i.e.,

$$\underline{c}^{n+1} = \underline{c}^{n} + \Delta t \begin{pmatrix} D_{11}L & 0 \\ 0 & D_{22}L \end{pmatrix} \underline{c}^{n+1} + \Delta t \begin{pmatrix} 0 & D_{12}L \\ D_{21}L & 0 \end{pmatrix} \underline{c}^{n}. \tag{35}$$

This time integration can be represented by

$$\underline{c}^{n+1} = \left(I - \Delta t \begin{pmatrix} D_{11}L & 0 \\ 0 & D_{22}L \end{pmatrix} \right)^{-1} \left(I + \Delta t \begin{pmatrix} 0 & D_{12}L \\ D_{21}L & 0 \end{pmatrix} \right) \underline{c}^{n} =: A\underline{c}^{n}. \tag{36}$$

Let r and $\underline{w}$ be an eigenvalue and eigenvector of the above matrix, then we consider

$$\left(I - \Delta t \begin{pmatrix} D_{11}L & 0 \\ 0 & D_{22}L \end{pmatrix} \right)^{-1} \left(I + \Delta t \begin{pmatrix} 0 & D_{12}L \\ D_{21}L & 0 \end{pmatrix} \right) \underline{w} = r\underline{w}. \tag{37}$$

For stability of the IMEX method, we need $|r| < 1$, and the above equation can be written as a generalized eigenvalue problem

$$\left(I + \Delta t \begin{pmatrix} 0 & D_{12}L \\ D_{21}L & 0 \end{pmatrix} \right) \underline{w} = r \left(I - \Delta t \begin{pmatrix} D_{11}L & 0 \\ 0 & D_{22}L \end{pmatrix} \right) \underline{w}. \tag{38}$$

We denote an eigenvector of L with eigenvalue λ by $\underline{v}$. In order to find solutions of the generalized eigenvalue problem (38), we try $\underline{w} = (\underline{v}\ \beta\underline{v})^{\mathrm{T}}$. Since L is symmetric its eigenvectors form a basis for $\mathbb{R}^n$, i.e., it is complete, and since $A \in \mathbb{R}^{2n\times 2n}$ the set of eigenvectors $\underline{w}$ represents a basis for $\mathbb{R}^{2n}$ if there are two distinct values for β for each eigenvector $\underline{v}$. Note that

$$\left(I + \Delta t \begin{pmatrix} 0 & D_{12}L \\ D_{21}L & 0 \end{pmatrix} \right) \begin{pmatrix} \underline{v} \\ \beta\underline{v} \end{pmatrix} = \begin{pmatrix} (1 + \Delta t D_{12}\lambda\beta)\underline{v} \\ (\beta + \Delta t D_{21}\lambda)\underline{v} \end{pmatrix} \tag{39}$$

and similarly

$$\left(I - \Delta t \begin{pmatrix} D_{11}L & 0 \\ 0 & D_{22}L \end{pmatrix} \right) \begin{pmatrix} \underline{v} \\ \beta\underline{v} \end{pmatrix} = \begin{pmatrix} (1 - \Delta t D_{11}\lambda)\underline{v} \\ (\beta - \Delta t D_{22}\lambda\beta)\underline{v} \end{pmatrix}. \tag{40}$$

We search β such that the right-hand side of Eq. (40) is a multiple of the right-hand side of (39), here this multiple defines the eigenvalue r, hence,

$$r = r(\lambda\Delta t) = \frac{1 + \Delta t D_{12}\lambda\beta}{1 - \Delta t D_{11}\lambda} \quad \text{and} \quad r = r(\lambda\Delta t) = \frac{\beta + \Delta t D_{21}\lambda}{\beta - \Delta t D_{22}\lambda\beta}. \tag{41}$$

The above equations give a quadratic equation for β with solutions

$$\beta_{\pm}(\xi) = \frac{D_{22} - D_{11} \pm \sqrt{(D_{12} - D_{22})^2 + 4D_{12}D_{21}(1 + \xi D_{22})(1 + \xi D_{11})}}{2D_{12}(1 + \xi D_{22})}, \tag{42}$$

where we set $\xi := -\lambda\Delta t > 0$ for ease of notation. Since $\beta_\pm$ stays bounded as $\xi \to 0$, we see from Eq. (41) that $r \to 1$ as $\xi \to 0$. Furthermore, since

$$\lim_{\xi\to\infty} |\beta_\pm| = \sqrt{\left|\frac{D_{21}D_{11}}{D_{12}D_{22}}\right|},$$

it follows that:

$$\lim_{\xi\to\infty} |r| = \sqrt{\frac{|D_{12}D_{21}|}{D_{11}D_{22}}} < 1 \quad \text{if and only if } |D_{12}D_{21}| < D_{11}D_{22}. \tag{43}$$

Note that the last inequality is also a necessary and sufficient condition for $\Re(\mathrm{eig}(D)) > 0$, which is necessary and sufficient for an analytically stable system. In the further discussion we will consider the following four cases: $0 < D_{12}D_{21} < D_{11}D_{22}$, $0 < D_{11}D_{22} < D_{12}D_{21}$, $0 < -D_{12}D_{21} < D_{11}D_{22}$ and $0 < D_{11}D_{22} < -D_{12}D_{21}$.

- First, we deal with $D_{12}D_{21} > 0$. Since $\xi > 0$, we have from Eq. (42) that $\beta_\pm \in \mathbb{R}$. Now, we search ξ such that

$$|r| = 1, \quad \text{i.e., } (1 - \xi D_{12}\beta_\pm)^2 = (1 + \xi D_{11})^2. \tag{44}$$

  Note that $\beta_\pm$ is a function of ξ (see Eq. (42)). The roots of the above equation are given by

$$\xi \in \left\{0, \frac{-(D_{11} + D_{22}) \pm \sqrt{(D_{11} + D_{22})^2 - 4(D_{11}D_{22} - D_{12}D_{21})}}{D_{11}D_{22} - D_{12}D_{21}}\right\}. \tag{45}$$

  The first root $\xi = 0$ is not interesting.
- Next, we treat two possibilities: $0 < D_{12}D_{21} < D_{11}D_{22}$ and $D_{12}D_{21} > D_{11}D_{22} > 0$:

  1. In the case that, besides $D_{12}D_{21} > 0$, we have $D_{21}D_{12} < D_{11}D_{22}$, then the last two roots are negative or complex-valued since $D_{11}D_{22} - D_{12}D_{21} > 0$. Using (43) for this case we always have $|r| < 1$ and hence the IMEX method is unconditionally stable. The roots in Eq. (45) apply for all real-valued cases.
  2. In the case that $0 < D_{11}D_{22} < D_{12}D_{21}$, then one of the eigenvalues of D is negative. This implies that the diffusion problem (1) is unstable with respect to perturbations. Hence we do not study the stability properties of the numerical method for this case.

- Next, we consider the case that $D_{12}D_{21} < 0$, then $\beta_\pm \in \mathbb{R}$ for small values of ξ, whereas for sufficiently large values of ξ we have $\beta_\pm \notin \mathbb{R}$. The real-valued case can be treated as in the preceding paragraph. Again we search ξ such that $|r| = 1$, taking into account that possibly $\beta_\pm \notin \mathbb{R}$. Therefore, we rewrite (41) as

$$|r|^2 = \frac{1 - 2\xi D_{12}\Re(\beta) + \xi^2|\beta|^2}{(1 + \xi D_{11})^2} = 1. \tag{46}$$

The real part and modulus of $\beta_\pm$ follow easily from Eq. (42). All parameters in the above equation are real-valued. A solution by MAPLE of Eq. (46) reveals that

$$\xi \in \left\{0, -\frac{D_{11}+D_{22}}{D_{11}D_{22}+D_{12}D_{21}}\right\}.$$

Note that the roots for the case of a real-valued β also apply, however, these roots are not treated here since they give nonpositive values for ξ. The first root is not interesting, however, the second root is positive if and only if $|D_{12}D_{21}| > D_{11}D_{22}$ and $D_{12}D_{21} < 0$. This implies the following criterion for stability if $-D_{12}D_{21} > D_{11}D_{22}$:

$$\xi < -\frac{D_{11}+D_{22}}{D_{11}D_{22}+D_{12}D_{21}}.$$

- Further, it can be seen that if $|D_{12}D_{21}| < D_{11}D_{22}$, then, there is no positive root and hence the method is unconditionally stable and super stable.

This is summarized in the following theorem.

Theorem 1. *Consider the time integration of Eq.* (26) *with fixed boundaries, and let* λ *be an eigenvalue of the discretized Laplace operator whose eigenvalues are all negative,* $D \in \mathbb{R}^{2\times 2}$ *and* D_{11}, $D_{22} > 0$, *and let* $\Re(\mathrm{eig}(D)) > 0$, *then*;

1. *The explicit time integration is stable if*

$$\Delta t < \frac{2\Re(\mathrm{eig}(D))}{|\lambda||\mathrm{eig}(D)|^2}, \quad \forall \lambda \in \mathrm{Spec}(L).$$

2. *The implicit time-integration is unconditionally stable and super stable.*
3. *If* $0 < |D_{12}D_{21}| < D_{11}D_{22}$ *then the IMEX time-integration, given by Eq.* (35), *is unconditionally stable and super stable. If* $|D_{12}D_{21}| > D_{11}D_{22}$ *then the IMEX time-integration is stable if* $D_{12}D_{21} < 0$ *and*

$$|\lambda|\Delta t < -\frac{D_{11}+D_{22}}{D_{11}D_{22}+D_{12}D_{21}} \quad if\ \ D_{12}D_{21} < 0, \quad \forall\ \mathrm{Spec}(L)$$

and if $0 < D_{11}D_{22} < D_{12}D_{21}$ *the* (*continuous*) *Eq.* (1) *is unstable*.

As a consequence of the above assertion one can prove the following statements:

Corollary 1. *Let all hypotheses in Theorem* 1 *be satisfied, then*

1. *For all discretizations with a symmetric matrix, Theorem* 1 *holds*.
2. *A consequence of Theorem* 1 *is that the IMEX time integration is unconditionally stable if the diffusion matrix is diagonally dominant and if the discretized Laplacian is symmetric*.

Numerical experiments with fixed boundaries reveal that the derived criterion in Theorem 1 is sharp.

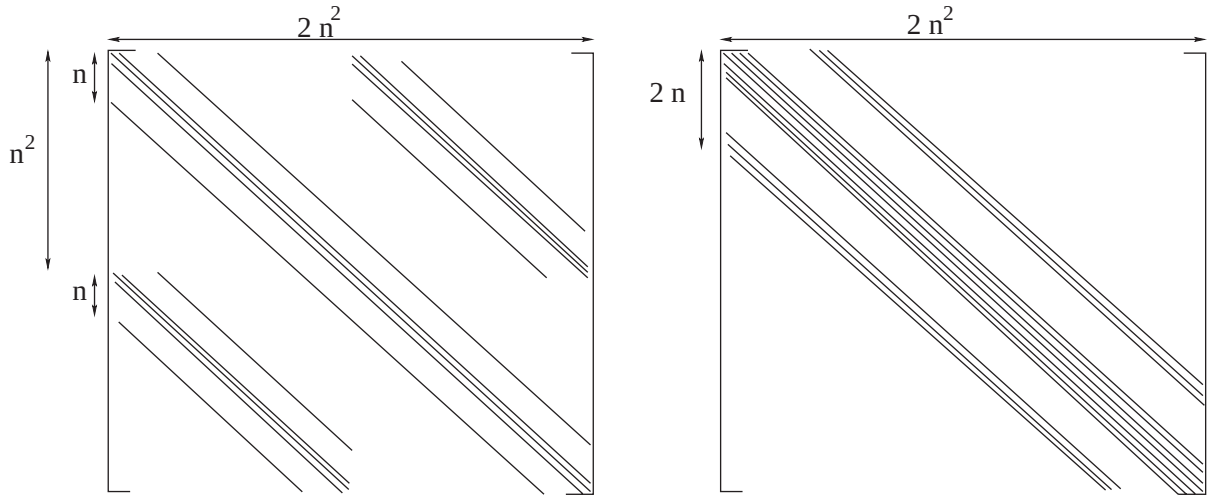

Fig. 1. Left: The nonzero elements of the overall discretization matrix for the implicit method for the straightforward arrangement of the unknowns as in Theorem 1. Right: The nonzero elements of the overall discretization matrix for an alternative numbering as in Eq. (47).

4.2. Efficiency of the methods

We compare the diagonalization based method with the direct method qualitatively. The direct method is split into either an IMEX time integration, which is conditionally stable under certain circumstances, or a fully implicit time integration, which is unconditionally stable. A straightforward arrangement as used for the proof of Theorem 1 gives a large discretization matrix for the fully implicit method when the direct method without diagonalization is used: Let $\underline{c} = \begin{pmatrix} \underline{c}_1 \\ \underline{c}_2 \end{pmatrix}$, then

$$\underline{c}^{j+1} = \underline{c}^{j} + \Delta t \begin{pmatrix} D_{11}L & D_{12}L \\ D_{21}L & D_{22}L \end{pmatrix} \underline{c}^{j+1},$$

where $\underline{c}_1$ and $\underline{c}_2$ represent the vectors with the unknown concentration at the gridnodes for c_1 and c_2. Hence, if (for two-dimensional cases) $L \in \mathbb{R}^{n^2 \times n^2}$, where n is the number of gridnodes in one spatial direction, then the discretization matrix consists of $2n^2 \times 2n^2$ entries, i.e., $A \in \mathbb{R}^{2n^2 \times 2n^2}$. The discretization matrix becomes four times as large as the discretized Laplacian. Further, if a straightforward arrangement of the unknowns is used, then the bandwidth increases considerably and the overall discretization matrix for two spatial co-ordinates roughly obtains the shape as in Fig. 1 for the case of a square domain of computation in $\mathbb{R}^2$. This matrix has a bandwidth of order $n^2 + n$, instead of order n which we would have for the discretized Laplacian. If we include more than two chemical species, then the situation gets worse: the bandwidth would become $n_s n^2 + n$, if n_s is the number of chemical species. Furthermore, for more spatial co-ordinates it also gets worse.

If the IMEX time integration is used, then the matrix equations can be solved separately. Hence the discretization matrices just become $\mathbb{R}^{n^2 \times n^2}$, and have the same sparsity structure as the discretized Laplacian with bandwidth of order n. For a two-dimensional situation a direct solution method for the

matrix equation is still useful. From an efficiency point of view for the fully implicit time integration with a straightforward arrangement of the unknown, we remark for the two-dimensional case that the matrix contains $2n^2$ columns and a bandwidth of $2(n^2+n)+1$ and hence the number of memory allocations is $2n^2(2(n^2+n)+1)-(n^2+n)(n^2+n+1)\approx 3n^4$ and the number of required flops becomes $2(2n^2(2(n^2+n)+1)-(n^2+n)(n^2+n+1)\approx 6n^4$ for the solution of the linear system of discretized equations.

For the IMEX time integration method the solution of the linear system takes $n^2(2n+1)-n(n+1)\approx 2n^3$ memory allocations and $2\times(n^2(2n+1)-n(n+1))\approx 4n^3$ flops. This implies that the IMEX time integration is more efficient than the implicit method with the straightforward arrangement of the unknowns. This holds, in particular, if the diffusion matrix is diagonally dominant, which is true in most of the metallurgical applications because then the IMEX method is unconditionally stable.

We remark here that a different arrangement of the unknowns in the concentration vector and discretization matrix is attractive for the implicit method. The solution vector can be rearranged into

$$\underline{c}=(c_{1,1},c_{2,1},c_{1,2},c_{2,2},\ldots,c_{1,n^2},c_{2,n^2})^{\mathrm{T}} \tag{47}$$

and the overall discretization matrix is as shown in Fig. 1 for the case of a square domain of computation in $\mathbb{R}^2$. Then, it can be verified that the LU-decomposition requires $2n^2(2(2n+1)+1)-(2n+1)(2n+2)\approx 8n^3$ memory allocations and $2[2n^2(2(2n+1)+1)-(2n+1)(2n+2)]\approx 16n^3$ flops for the solution of the linear system, which is favorable over the straightforward arrangement, but still more work than the IMEX method. Here the number of diagonals with nonzero entries is 11. If we consider n_s species, then the number of nonzero diagonals becomes $5n_s+1$ for $n_s\geqslant 2$ if a square geometry in $\mathbb{R}^2$ is considered.

If the diagonalization argument is used then approximately the same number of memory allocations and flops are required for the IMEX and implicit time integration methods. Further an implicit method guarantees numerical stability. If D depends on time then at each timestep the eigenvalues and eigenvectors of D and the transformations of the concentrations $\underline{u}\rightarrow\underline{c}$ and $\underline{c}\rightarrow\underline{u}$ at each gridnode have to be determined. However, if D also depends on position, or on the concentration itself, then diagonalization can no longer be used. For this case one can rely on the IMEX time-integration. The same efficiency remarks as for the implicit method hold for a Crank–Nicholson time-integration for the direct method without diagonalization. Some quantitative results based on numerical experiments will be presented in Section 5.

5. Numerical experiments

In this section, we compare the performance of several numerical techniques. First, we distinguish between the IMEX and Euler backward time integration methods for the coupled set of equations. For both time integrations we analyze the performance of the Newton and Picard iterations to solve the nonlinear problem. Finally, we compare these solutions with those that were obtained by the use of the diagonalization argument. As a test-problem we take

$$D=\begin{pmatrix}1 & -0.25\\ -0.25 & 2\end{pmatrix},\quad \underline{c}^p=\begin{pmatrix}50\\50\end{pmatrix},\quad c_1^{\mathrm{sol}}c_2^{\mathrm{sol}}=1,\quad \underline{c}^0=\begin{pmatrix}0\\0\end{pmatrix}$$

and $S(0)=1$, $0\leqslant S(t)\leqslant x\leqslant 10$. For a study on the impact of the off-diagonal terms of the diffusion matrix on the evolution of the moving interface, we refer to [21]. For the above configuration the IMEX time

Table 1
CPU-times for the numerical solution of the nonlinear problem for a grid of 50 gridnodes

Method/convergence	$\Delta t = 0.01$	$\Delta t = 0.1$	$\Delta t = 1$
IMEX–Newton	122	12.1	—
IMEX–Picard	25.0	3.36	—
IMEX–Picard (0.5)	24.35	3.47	1.33[a]
IMEX–Picard (1.5)	71.29	3.13	—

[a]Inaccurate solution.

integration of the concentration profiles should be unconditionally stable with respect to the time-step according to Theorem 1. The calculations that we present are done for the vector Stefan problem with one spatial co-ordinate unless stated otherwise. Finally, we illustrate the importance of cross-diffusion for the dissolution of system from literature.

5.1. The IMEX time integration

Note that the proof of Theorem 1 has been given for the case that the interface position does not change in time. In the experiments of this section we allow the interface to move. From the numerical simulations it turns out that convergence to the solution of the nonlinear problem depends on the choice of the time-step and the grid-size. In Table 1, we present the matlab CPU time for the Newton, Picard (with and without relaxation) for time-steps $\Delta t = 0.1$ and 1. The CPU-time is taken at $t = 100$. The number of iterations is for the numerical solution of the nonlinear problem at the second time-step. The numbers 0.5 and 1.5 denote the value of ω used in the relaxated Picard method.

From Table 1 it can be seen that Newton's method takes most CPU-time. This is caused by the fact that for each time iteration we need to evaluate the concentration profiles five times. Further, it turns out that the IMEX method performs badly when the time-step is chosen very large $\Delta t = 1 \gg (\Delta x)^2$. The minus-bars for $\Delta t = 1$ in Table 1 denote that the method did not converge (for the Picard method) or converged to a wrong solution (in the case of Newton iterations). Convergence to the wrong solution in the Newton case could not be avoided by the choice of a better initial guess for the interface concentrations. The bad convergence behavior of the Picard method when $\Delta t = 1$ is caused by the spectral radius of the Jacobian of the function $\underline{g}$, which is larger than one. We remark that the solution can be determined numerically for large Δt by means of relaxation of Picard's method. However, we recommend here to choose a small time-step Δt instead, since it is not easy to obtain an optimal choice for ω for different values of Δt and Δx.

To have a closer look at the influence of the moving boundary and the nonlinear boundary condition for the interface concentrations on the numerical stability as in Theorem 1, we consider the following example with $D = \begin{pmatrix} 3 & 3 \\ -3 & 2 \end{pmatrix}$. For this case, we have $D_{12}D_{21} > D_{11}D_{22} > 0$ and hence Theorem 1 gives the following criterion for stability: $|\lambda|\Delta t < \frac{5}{3}$. The other variables have the same value as in the previous calculations. Having 50 gridnodes and a $\Delta t = 0.01$, we obtain that $\max |\lambda|\Delta t \approx 1.2582$ and hence we are within the derived stability criterion for the problem with the fixed boundaries. Taking $c_1^{\text{part}} = c_2^{\text{part}} = 2$ or larger values, then, the obtained numerical solution is stable. However, for lower values of the particle concentrations, say $c_{1,2}^{\text{part}} = 1.15$, the solution becomes unstable. Here the movement of the boundary

Table 2
CPU-times for the numerical solution of the nonlinear problem for a grid of 50 gridnodes

Method/convergence	$\Delta t = 0.01$	$\Delta t = 0.1$	$\Delta t = 1$
Euler backward–Newton	892	88.9	8.88
Euler backward–Picard	41.1	4.41	1.15
Euler backward–Picard (0.5)	199	20.9	3.61
Euler backward–Picard (1.5)	483	13.9	2.14

increases rapidly. By choosing a smaller time-step the numerical solution becomes stable again. We remark here that the eigenvalues of the diffusion matrix in this case are complex-valued.

We observed that if the difference between the particle concentrations and the interface concentrations is large, then, the bound in Theorem 1 is reliable also for the moving boundary problem. This is due to the slow movement of the interface for this case. From this we conclude that the stability criterion in Theorem 1 serves as a necessary condition for the complete moving boundary problem, which is sharp in the limit as the interface velocity tends to zero.

5.2. The Euler backward time integration

We remark that this method is unconditionally stable, see Theorem 1. In Table 2 we present the number of iterations for the solution of the nonlinear problem and CPU-time for the Newton, Picard (with relaxation) methods for time-steps $\Delta t = 0.01$, 0.1 and 1. The CPU-time is at $t = 100$. Further the straightforward arrangement of the unknowns is used in the calculations of this subsection.

From Table 2 we see that Picard's method is faster than the Newton method. This agrees with the observation for the IMEX time-integration. Further, we see that for $\Delta t = 0.1$ the IMPLICIT method takes more CPU-time than the IMEX scheme. However, for large time-steps it turns out that the Euler backward method is more reliable than the IMEX method. Picard (without relaxation) seems to give the best results. For reasons of robustness the IMPLICIT method is favorable over the IMEX method. However, for CPU-time and small time-step we prefer to use the IMEX method.

5.3. IMEX and Euler backward methods for 2D problems

From the above it seems that the Euler backward method is advantageous. Since we intend to extend the models to more spatial dimensions as well, we present some CPU-times for 10 time-iterations for two-dimensional diffusion equations. The discretization is done on an equidistant grid with the use of Finite Volumes. Furthermore, the values of the interfacial concentrations are prescribed $c_1^{\mathrm{sol}} = 1 = c_2^{\mathrm{sol}}$ and the boundaries are fixed. The calculations are done by the use of an IMEX and Euler backward time integration based on the straightforward arrangement of the unknowns. The linear system of equations has been solved by Gaussian elimination for all cases. The results are presented in Table 3.

From Table 3 it can be seen that the IMEX method requires less CPU-time than the Euler backward method. The difference increases as the number of gridnodes increases. This is in agreement with the expectations as given in Section 4. For three-dimensional problems with many more gridnodes, this difference is expected to increase. Hence, for small time-steps, we prefer the use of the IMEX method.

Table 3
Calculation times for 10 time iterations ($\Delta t = 10$)

Method/grid	25×25	50×50	100×100	200×200
IMEX	0.15	0.85	5.77	46.6
Euler backward	0.28	1.69	14	117

Table 4
CPU-times for the numerical solution of the nonlinear problem for a grid of 50 gridnodes

Method/convergence	$\Delta t = 0.01$	$\Delta t = 0.1$	$\Delta t = 1$
DIAG–Newton	113	11.2	1.12
DIAG–Picard	24.1	2.94	1.01
DIAG–Picard (0.5)	24.1	3.00	1.17
DIAG–Picard (1.5)	24.1	3.01	0.88

5.4. Use of diagonalization of the diffusion matrix

We use the Euler backward and remark that this method is unconditionally stable due to the decoupling of the diffusion equations. The CPU-times and number of iterations are listed in Table 4.

We see from Table 4 that Picard's method gives the shortest CPU-time. Further, we see that this method is efficient (shortest computation times for both $\Delta t = 0.1$ and 1) and robust. This agrees with the expectations as predicted for the linear diffusion system in Section 4.

5.5. An industrial example

As an industrial example we take the dissolution of an Al_2CuMg particle in aluminum for which the cross-diffusion coefficients are known. For the data we refer to [7]. This example was also treated, incorporating cross-diffusion, by Vusanovic et al. [24]. A similar model as here is described there, however, a mathematical and numerical analysis and description of the used method are not given there. We take a rectangular geometry with initial particle size 0.2 μm and the diffusion matrix is given by (in $\mu m^2/s$):

$$D = \begin{pmatrix} 0.051 & -0.034 \\ -0.0077 & 0.151 \end{pmatrix}.$$

The particle concentrations are given by $c_{\mathrm{Cu}}^{\mathrm{part}} = 33$ wt% and $c_{\mathrm{Mg}}^{\mathrm{part}} = 6$ wt%. In the above diffusion matrix element 1 and 2, respectively, correspond to copper and magnesium. Due to lack of data-points some discrete values for the solubility line in the aluminum rich corner are used instead of Eq. (5). The initial concentrations were taken zero and the cell radius is 10 μm. The results are shown in Figs. 2 and 3 where we plot the concentration profiles in the vicinity of the moving boundary and the interface position, respectively. In both figures we notice the significance of cross-diffusion. Since the cross-terms in the diffusion matrix are negative, the dissolution is slowed down significantly due to cross-diffusion (see Fig. 3) although the concentration profiles do not differ too much (see Fig. 2).

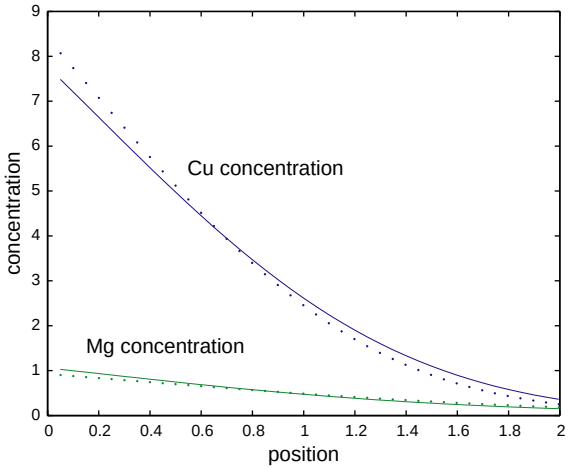

Fig. 2. Concentration profiles at $t = 20\,\mathrm{s}$ during dissolution of a Al_2CuMg particle in aluminum. The dotted lines represent the concentration profiles with the incorporation of cross-diffusion.

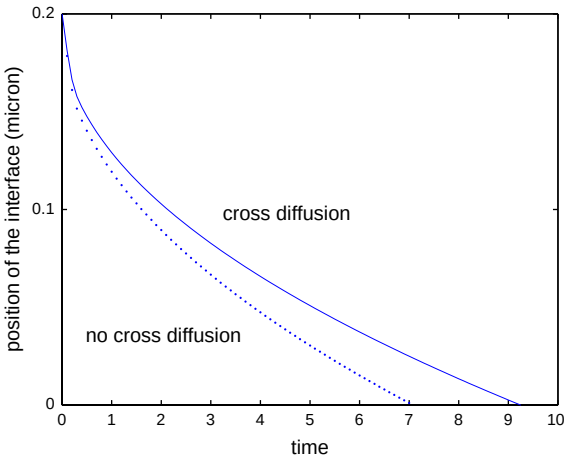

Fig. 3. The interface position as a function of time during dissolution of a Al_2CuMg particle in aluminum. The dotted line represents the concentration profiles with the incorporation of cross-diffusion.

6. Conclusions

We analyzed several numerical methods for the cross-diffusion problem with a moving interface. We study the Euler backward time integration method, which is proven to be unconditionally stable for the linear cross-diffusion equation. This method turns out to be very robust when it is used in the solution of the nonlinear system to determine the interfacial concentrations. A drawback is the long computation time needed to solve the large system of linear equations from the spatial discretization. This becomes worse as the dimensionality of the problem increases. The IMEX time-integration method to integrate the concentration profiles with fixed boundaries as a function of time is conditionally stable under the

circumstance that $-D_{12}D_{21} > D_{11}D_{22} > 0$ and for other cases the method is unconditionally stable. However, it turns out the method is less robust when a large time-step is used. This suggests that the derived stability criterion of the IMEX time integration method for fixed boundaries serves as a necessary condition for the complete vector-valued Stefan problem. Although, the computation times are less than for the fully implicit method. If diagonalization is used then the IMEX and Euler backward time-integration methods are equivalent. Then, stability is guaranteed for the linear diffusion equation and the discretization matrix has the same sparsity pattern as the discretized Laplacian. Hence, the method is efficient. If the diffusion matrix is not constant over the domain of computation (such as for nonlinear diffusion), then the diagonalization argument is no longer applicable. Further, if the diffusion matrix depends on time only, then the diagonalization has to be carried out at each time-step. Since D is a small sized matrix in general, this does not restrict its applicability.

Therefore as our main conclusion we recommend the use of the diagonalization argument if D is a constant matrix over the domain.

Acknowledgements

We wish to express our gratitude to prof.dr.ir. S. van der Zwaag from the Department of Aerospace Engineering at the Delft University of Technology for drawing our attention to this problem. Further, we like to thank one of the referees for his suggestions which improved the manuscript considerably.

References

[1] C. Atkinson, T. Akbay, R.C. Reed, Theory for reaustenization from ferrite/cementite mixtures in Fe–C–X steels, Acta Mater. 43 (5) (1995) 2013–2032.
[2] G. Birkhoff, S. MacLane, A Survey of Modern Algebra, Macmillan, New York, 1953.
[3] J. Chadam, H. Rasmussen, Free Boundary Problems Involving Solids, Longman, Scientific & Technical, Harlow, 1993.
[4] S. Chen, B. Merriman, S. Osher, P. Smereka, A simple level-set method for solving Stefan problems, J. Comput. Phys. 135 (1997) 8–29.
[5] J. Crank, Free and Moving Boundary Problems, Clarendon Press, Oxford, 1984.
[6] C.M. Elliot, J.R. Ockendon, Weak and Variational Methods for Moving Boundary Problems, Pitman Advanced Publishing Program, Boston, London, Melbourne, 1982.
[7] W.F. Gale, T.C. Totemeier, Smithells Metals Reference Book, eighth ed., Elsevier Butterworth-Heinemann, Amsterdam, 2004.
[8] U. Grafe, B. Böttger, J. Tiaden, S.G. Fries, Coupling of multicomponent thermodynamics to a phase field model: application to solidification and solid-state transformations of superalloys, Scripta Mater. 42 (2000) 1179–1186.
[9] E. Javierre-Perez, Literature study: numerical methods for solving Stefan problems, Technical report at the Delft University of Technology, Department of Applied Mathematical Analysis, TWA-03-16, 2003.
[10] J.S. Kirkaldy, D.J. Young, Diffusion in the Condensed State, The Institute of Metals, London, 1987.
[11] R. Kobayashi, Modeling and numerical simulations of dendritic crystal growth, Phys. D 63 (1993) 410–423.
[12] P. Lancaster, Theory of Matrices, Second ed., Academic Press, Orlando, 1985.
[13] A.M. Meirmanov, M. Niezgodka, A. Crowley, The Stefan Problem, Walter de Gruyter, Berlin, 1992.
[14] W.D. Murray, F. Landis, Numerical and machine solutions of transient heat conduction problems involving freezing and melting, Trans. ASME (C), J. Heat Transfer 245 (1959) 106–112.
[15] E.B. Naumann, J. Savoca, An engineering approach to an unsolved problem in multi-component diffusion, AICHE J. 47 (5) (2001) 1016–1021.

[16] S. Osher, J.A. Sethian, Fronts propagating with curvature-dependent speed: algorithms based on Hamilton–Jacobi formulations, J. Comput. Phys. 79 (1988) 12–49.
[17] O. Reiso, N. Ryum, J. Strid, Melting and dissolution of secondary phase particles in AlMgSi-alloys, Metall. Trans. A 24A (1993) 2629–2641.
[18] F.J. Vermolen, C. Vuik, A numerical method to compute the dissolution of second phases in ternary alloys, J. Comput. Appl. Math. 93 (1998) 123–143.
[19] F.J. Vermolen, C. Vuik, A mathematical model for the dissolution of particles in multi-component alloys, J. Comput. Appl. Math. 126 (2000) 233–254.
[20] F.J. Vermolen, C. Vuik, Numerical solution of vector Stefan problems with cross-diffusion, in: P. Neitaanmäki, T. Rossi, S. Korotiv, E. Onate, J. Periaux, D. Knötzer Jyväskylä (Eds.), European Congress on Computational Methods in Applied Sciences and Engineering, ECCO-MAS 2004, Finland, 2004.
[21] F.J. Vermolen, C. Vuik, S. van der Zwaag, Particle dissolution and cross-diffusion in multi-component alloys, Mater. Sci. Eng. A 347 (2003) 265–279.
[22] F.J. Vermolen, C. Vuik, S. van der Zwaag, Diffusion controlled particle dissolution and cross-diffusion in metallic alloys, Comput. Vis. Sci. (2004) accepted.
[23] A. Visintin, Models of phase transitions, Progress in Nonlinear Differential Equations and their Application, vol. 38, Birkhauser, Boston, 1996.
[24] I. Vusanovic, D. Voronjec, M.J.M. Krane, Microsegregation phenomena in AlCuMg alloy with considering of diffusion phenomena in primary phase, Facta Univ. Series Mech. Eng. 1 (8) (2001) 965–980. http://facta.junis.ni.ac.yu/facta/me/me2001/me2001-05.pdf